PERGAMON

International Journal of Heat and Mass Transfer 42 (1999) 2053–2062

International Journal of HEAT and MASS TRANSFER

Heat transfer enhancement due to self-sustained oscillating transverse vortices in channels with periodically mounted rectangular bars

A. Valencia*

Departamento de Ingeniería Mecánica, Universidad de Chile, Casilla 2777, Correo 21 Santiago, Chile

Received 3 February 1998; in final form 18 August 1998

Abstract

Numerical investigations of flow structure and heat transfer in a channel with periodically mounted transverse vortex generators (bars) have been conducted in the Reynolds number range of steady laminar to oscillatory transitional flow. The unsteady Navier–Stokes equations and the energy equation have been solved by a finite volume code. Due to the periodic geometry, instability leads at relatively low Reynolds number to self-sustained oscillations and vortex shedding from the bars. At Reynolds number $Re = 150$, the flow structure is already time periodic. With increasing Reynolds number their amplitudes and number of frequencies increase. The data for heat transfer and flow losses are presented for different periodicity lengths in a Reynolds number range of 100–400.

Nomenclature

C_f skin friction coefficient, $\tau_w/(1/2\rho U_0^2)$
C_d drag coefficient on the bar, $D/(1/2\rho U_0^2 h)$
D drag [N m^{-1}]
f friction factor, $(H/2L)\Delta p/(1/2\rho U_0^2)$; also eddy shedding frequency [1 s^{-1}]
h bar height [m]
h_x local heat transfer coefficient [W m^{-2} K^{-1}]
H channel height [m]
k thermal conductivity of bar [W m^{-1} K^{-1}]
k_0 thermal conductivity of air [W m^{-1} K^{-1}]
l bar length [m]
L periodicity length [m]
Nu_x local Nusselt number, equation (8)
Nu average Nusselt number
p pressure [Pa]
P non-dimensional pressure, $p/\rho U_0^2$
Pr Prandtl number, v/α
Re channel Reynolds number, $U_0 H/v$
S Strouhal number, fH/U_0
T temperature [K]
T_0 reference temperature [K]
T_W channel wall temperature [K]
T_B bulk temperature [K], equation (7)
u Cartesian velocity component in the x-direction [m s^{-1}]
v Cartesian velocity component in the y-direction [m s^{-1}]
U_0 channel-averaged velocity at the inlet [m s^{-1}]
U non-dimensional Cartesian velocity component, u/U_0
V non-dimensional Cartesian velocity component, v/U_0
X non-dimensional Cartesian coordinate, x/H
Y non-dimensional Cartesian coordinate, y/H.

Greek symbols
α thermal diffusivity [m^2 s^{-1}]
β mean pressure gradient, equation (5)
Δ difference
ϕ dimensionless pumping power
θ non-dimensional temperature, T/T_0
v kinematic viscosity [m^2 s^{-1}]
τ non-dimensional time, tU_0/H
τ_w wall shear stress [N m^{-2}].

1. Introduction

Heat transfer enhancement in fluid flows is often obtained by geometric modifications or structures of the

* Tel.: 0056 2 6988453; fax: 0056 2 6988453; e-mail: alvalenc@tamarugo.cec.uchile.cl

0017–9310/99/$ - see front matter
PII: S0017–9310(98)00295–6

wall. These modifications induce vortices to augment transverse fluid mixing and to reduce the thermal boundary layer thickness. Particular types of modifications allow control of generation and orientation of vortices. Principally transverse vortices and longitudinal vortices can be distinguished. Transverse vortices have their axes transverse to the flow and are consistent with two-dimensional flow, while longitudinal vortices have their axes along the flow mainly in the streamwise direction and imply three-dimensional flow.

For internal flow, relatively few investigations have been made on the generation of vortices and their influence on flow structure and heat transfer. These have included longitudinal vortex generators in the form of winglets on the channel surface, and transverse vortex generators as cylinders, rectangular bars or grooved channels. Ribs, offset-strip fins, louver fins and corrugations in channels also induce transverse vortices. An extensive coverage of the application of vortex generators for compact heat exchangers is given by Fiebig [1].

Although some additional space may be required to place a vortex generator in the channel, the technique is passive, economical and does not cause any undue vibrations or noise in the system. However, the beneficial effect of a vortex generator is maximized only if it is optimally spaced in the channel. This sensitivity of thermal performance to geometrical arrangement has spurred considerable interest in identifying optimal arrangements.

The Karman vortex street in the wake of a circular cylinder in cross flow is perhaps the most thoroughly investigated transverse vortex system. For Reynolds numbers, based on the cylinder diameter and the free stream velocity, between 50 and 170 the separation lines oscillate and shed alternate shear layers, which form into the transverse vortices of the Karman vortex street. When the Reynolds number is increased further three-dimensional instabilities are amplified and the wake becomes three-dimensional [2].

In a pioneer experimental work, Thomas [3] shows that the local and the average rates of forced convection through laminar boundary layers on a flat plate can be markedly increased by locating small cylinders near the outer edge of the boundary layer. The maximum increase in local Stanton number caused by the second cylinder was both substantially larger and more strongly dependent on velocity than was the maximum observed with the first or single cylinder.

Thomas [4] also investigated the increase of mass transfer in the wake region behind detached cylindrical turbulence promoters with the use of the naphthalene sublimation technique. The maximum increases in the average rate of mass transfer through laminar boundary layers was over 170%. The amplification of a disturbance in a laminar boundary layer is a function of both the initial amplitude and frequency of the disturbance. In the particular case of Tollmien–Schlichting waves, the maximum amplification factor is associated with lower frequency disturbances. The results of Thomas [4] are consistent with this observation. The wake from cylinders placed directly on a flat or slightly convex surface excites Tollmien–Schlichting waves and promotes early transition.

Kapat et al. [5] report on laminar-to-turbulent transition in a rectangular channel in the presence of periodically placed cylindrical eddy promoters. Placement of the eddy promoters in the channel, depending on the geometric configuration, can significantly reduce the value of Reynolds number at transition. The critical Reynolds number decreases, by more than a factor of three, from 1500 for plane channel to about 400 for the most unstable deployed configuration.

Karniadakis et al. [6] show that the addition of small cylinders in a plane channel results in stability modes that are little changed in form or frequency from plane-channel Tollmien–Schlichting waves. However, for eddy-promoter flow in which the cylinder is placed near the center of the channel, the instability-mode spatial structures are consistent with the Karman vortex street. In this case the vorticity generation at the channel walls next to the cylinders and on the cylinder surface is the most important fraction of the total vorticity generation in the system.

This destabilizing of the flow increases momentum transfer, with corresponding increases in the value of wall shear stress, and thus these flows yield heat transfer rates commensurate with those of a plane-channel turbulent flow but a much lower Reynolds number. Karniadakis et al. use a viscous dissipation parameter $\Phi = 3(\mathrm{d}p/\mathrm{d}x)Uh^4/4\rho\nu^3$ to show that the eddy-promoter flows can save a lot in pumping power for the same heat transfer as plane channel turbulent flows.

Recently Anand et al. [7] analyzed the periodic fully developed flow and heat transfer in a plane channel with rectangular bars placed in-line at the center of the channel. Based on pressure drop considerations, it was concluded that blockage ratios (height of bar/channel height) greater than 0.6 are not desirable. The above mentioned numerical study considered the flow to be steady. Thus, only the steady-state equations were solved. However, the assumption of steady flow in such periodically repeating channels appears to be questionable even at a modest Reynolds number.

The mixing between the core and boundary-layer fluids is increased by creating an unsteadiness in the transverse vortex either through natural transition or through external forcing of the inflow. Such self-sustained and forced oscillations are observed to increase considerably the rates of heat transfer in plane channels with different forms of transverse vortex generators.

Greiner [8] investigated resonant heat transfer in grooved channels. Flow pulsations were actively imposed

on the flow. The frequency of the pulsations was tuned to the natural frequency of the grooved channel flow and a further increase in heat transfer was observed.

For channels with periodic transverse ribs Grosse-Gorgemann et al. [9] have shown that self-sustained oscillations of transverse vortices generate several times the heat transfer of a plane channel for the same pumping power. In steady flows, transverse vortices generate local variations of heat transfer but no global enhancement.

Wang et al. [10] investigated the enhancement of heat transfer due to unsteady flow in channels with in-line and staggered ribs. For the in-line configuration, the flow becomes naturally unsteady at a critical Reynolds number around 110. For the staggered case, this value is around 200. Significant increases in heat transfer rate are reported once the flow becomes unsteady. In both configurations, a Hopf bifurcation is seen to occur at the first critical Reynolds number, leading to an unsteady time-periodic flow.

The mechanism of heat transfer enhancement due to self-sustained oscillation in communicating channels (thick colinear fins located in the mid-plane of the channel) was investigated by Amon et al. [11]. Flow instability generates a series of transverse vortices in the wake of the fins, leading to relatively thin thermal boundary layers that further contribute to heat transfer augmentation on the fins. They observed self-sustained oscillation at a critical Reynolds number which was lower than the critical Reynolds number of the corresponding plane channel flow. In the low Reynolds number range the frequency values closely follow the three-wave Tollmien–Schlichting solution for plane channel flow. Suzuki et al. [12] found that the flow instability produces dissimilarity between the momentum transfer and heat transfer. The phase shift induces a Reynolds stress, which is responsible for the increase in momentum diffusion and for converting energy from the basic mean flow to the oscillatory flow. Majumdar and Amon [13] also studied numerically the mechanism of heat transfer enhancement due to self-sustained oscillations in communicating channels. They analyzed the contribution of the fluctuating components of the velocity and pressure on the momentum transport.

Herman et al. [14] report experimental measurements of unsteady temperature distributions and local heat transfer in grooved and communicating channels. The Reynolds number in the communicating channels is defined as $Re_c = 3/2Uh/v$, where the characteristic length scale h in this definition represents the half-height of the main channel. The critical Reynolds number for the onset of oscillations was experimentally determined to be around 200, the flow is time-periodic and exhibits a single fundamental frequency. In the regime of higher Reynolds number the flow is quasiperiodic and it mostly exhibits two dominant frequencies. By analyzing sequences of interferometric images, different oscillatory regimes and varying oscillatory regimes were detected. The authors notice the presence of four and three traveling waves over the double periodicity length of the channel. As the flow structure in the communicating region is in agreement with the traveling wave structure in the main channels, the vortical structures in two successive communicating regions are either identical or antisymmetric respectively.

Zhang et al. [15] studied the heat transfer enhancement mechanisms and performance associated with interrupted surfaces in compact heat exchangers. They reported geometry effects such as finite fin thickness and a comparison between inline and staggered arrangements. Irrespective of fin arrangement the flow is observed to follow a sequence of transitions. At very low Reynolds number the flow is steady and above a critical Reynolds number, flow becomes unsteady with a single dominant frequency. At even higher Reynolds numbers an additional lower frequency is generated and with subsequent increase in Re the flow becomes chaotic. In the inline arrangement these transitions are observed at a higher Reynolds number than in the staggered arrangement. But in both arrangements the unsteady regime is marked by transverse vortices that are generated at the leading edges of the fin element, which travel down on the top and bottom surfaces of the fin element. These transverse vortices play a key role in significantly enhancing the local heat transfer by bringing fresh fluid from the freestream towards the fin surface. They also show in [16] that a higher Reynolds numbers, the additional effect introduced by the intrinsic three-dimensionality of the flow plays another important role in determining the total heat exchanger performance. At $Re = 2450$ the two-dimensional solution overpredicts the experimental Colburn factor by 17%.

Suzuki et al. [17] computed the unsteady laminar flow in a channel with a transverse vortex generator in the form of a square bar and found that the vortex street shows a different pattern of motion from its counterpart formed behind a bar placed in a uniform flow. The blockage ratio is indicated to be a major factor governing the conditions for the appearance of crisscross motion of the vortex.

Tatsutani et al. [18] showed that for the flow past a pair of bars of square cross-section placed in tandem, three distinct flow patterns as a function of the bar separation distance and Reynolds number exist: (i) the inter-bar flow consists of a pair of steady counter-rotating eddies; (ii) vertical flow oscillations arise in the inter-bar space and (iii) at a critical inter-bar spacing the shedding of large eddies also occurs at the upstream bar and this results in a highly mixed flow.

Valencia [19] presented a numerical study of the flow and heat transfer in a plane channel with a built-in tandem of rectangular bars. The numerical results reveal the oscillatory structure of the flow when the system is operated near a critical channel Reynolds number of about 200. Heat transfer enhancement on the channel

walls is about a factor 1.8 with bar separation distances greater than one channel height at $Re = 400$. For a bar separation distance of one, the heat transfer on the channel walls was only 8% higher than in a channel with one built-in rectangular bar. For steady flow the bar separation distance had no effect on heat transfer and different bar separation distances only change the flow losses.

In spite of these recent efforts, the influence of Karman transverse vortices on local heat transfer and pressure drop needs to be quantified in a channel with periodically mounted bars by high blockage ratios. A number of important issues regarding how these vortices interact with channel instabilities remain to be explored.

This work was undertaken to provide information on the unsteady flow and heat transfer processes in channels with periodically mounted transverse vortex generators and to quantify the beneficial effects of self-sustained oscillations. Calculations have been performed for several flow Reynolds numbers ranging from steady laminar to lower transitional region and for different periodicity lengths. The geometry represents a model of the rectangular plate fin flow passages of compact heat exchangers.

In the present study, the flow is assumed to be two-dimensional. This assumption is made primarily to keep the computational times manageable. Well-resolved three-dimensional computations will require considerably large CPU times to conduct parametric tests such as those conducted in this study. Thus, the effects of three-dimensionality, which may arise due to either secondary instabilities or end walls, were not considered. While geometrically simple, as will be shown, the configurations investigated give rise to highly complex flows.

2. Mathematical formulation

The flow and temperature fields are governed by the continuity, non-steady two-dimensional Navier–Stokes and energy equation. The fluid properties are assumed to be constant and the dissipation terms in the energy equation are neglected.

$$\frac{\partial U}{\partial X}+\frac{\partial V}{\partial Y}=0 \tag{1}$$

$$\frac{\partial U}{\partial \tau}+\frac{\partial U^2}{\partial X}+\frac{\partial UV}{\partial Y}=-\frac{\partial P}{\partial X}+\beta+\frac{1}{Re}\left(\frac{\partial^2 U}{\partial X^2}+\frac{\partial^2 U}{\partial Y^2}\right) \tag{2}$$

$$\frac{\partial V}{\partial \tau}+\frac{\partial UV}{\partial X}+\frac{\partial V^2}{\partial Y}=-\frac{\partial P}{\partial Y}+\frac{1}{Re}\left(\frac{\partial^2 V}{\partial X^2}+\frac{\partial^2 V}{\partial Y^2}\right) \tag{3}$$

$$\frac{\partial \theta}{\partial \tau}+\frac{\partial U\theta}{\partial X}+\frac{\partial V\theta}{\partial Y}=\frac{1}{RePr}\left(\frac{\partial^2 \theta}{\partial X^2}+\frac{\partial^2 \theta}{\partial Y^2}\right) \tag{4}$$

The velocity components have been non-dimensionalised with the average velocity U_0 and the length with the channel height H. Re is the Reynolds number and Pr is the Prandtl number.

The present numerical solutions will assume periodicity of the solution over one basic unit and therefore the actual computational geometry will be limited to this basic unit. Implicit in this treatment is the assumption that the flow is fully developed, both hydrodynamically and thermally, the thermal entrance effects were reported in [19] for a mounted tandem of rectangular bars.

To enable periodic boundary conditions, the instantaneous non-dimensional pressure p is decomposed into a mean part that is assumed to vary linearly in X and a fluctuating part that varies in X and Y [20, 21]. Thus:

$$p(X,Y,\tau) = -\beta(\tau)X + P(X,Y,\tau) \tag{5}$$

where β is the mean pressure gradient. This gradient is adjusted every time step to satisfy the fixed mass flow condition. Boundary conditions are imposed on intermediate velocities and on the fluctuating part of the pressure. This approach with periodic boundary conditions has been successfully extended to the study of unsteady flows in the literature, [9–11, 15].

The thermal boundary conditions are uniform channel walls temperature and the bar does not have imposed temperature, the thermal conductivity of the bar is k. A important difference to previous works is the thermal boundary condition on the vortex generator, in this work only the temperatures at the top and bottom channel walls are constant and are equal to $T_{w.}$ The redevelopment of the thermal boundary layer on interrupted surfaces has a significant impact on heat transfer enhancement, if the heating is applied to the vortex generator, the bar here only generates the transverse vortex and the heat transfer surface is the same as in a plane channel without bar.

For the periodic thermally developed domain, the temperature difference:

$$\frac{T(0,Y,\tau)-T_W}{T_B(0)-T_W}=\frac{T(L,Y,\tau)-T_W}{T_B(L,\tau)-T_W} \tag{6}$$

can be considered to be periodic along the X-direction. The periodicity condition (6) enables the solution domain for the temperature problem limited to the streamwise length L. This periodic thermally developed regime is a logical generalization of the conventional thermally developed regime [20].

The bulk temperature was calculated using the velocity and the temperature distribution with the equation:

$$T_B(x)=\frac{\int_0^H uT\,dy}{\int_0^H u\,dy} \tag{7}$$

Instantaneous local heat transfer will be expressed in

terms of the instantaneous local Nusselt number based on channel height and can be written as:

$$Nu_x = \frac{h_x H}{k_0} = \frac{(\partial T/\partial y)_{\text{wall}} H}{(T_B(x) - T_W)} \tag{8}$$

The flow losses are evaluated with the friction factor defined as:

$$f = C_f + C_d \frac{h}{2L} \tag{9}$$

Here the governing equations are solved with all the relevant length and time scales adequately resolved for the correct simulation of laminar and transitional unsteady flows.

3. Computational details

Figure 1 schematically shows the computational domain. The streamwise periodicity length of the domain L was varied, the computation was made for three non-dimensional periodicity lengths: $L/H = 2.25$, 4.25 and 6.25. The cylinder aspect ratio was $l/h = 0.5$ and the blockage ratio was $h/H = 0.5$.

The geometry of the bar was considered [22]. For the investigated bars: $h/H = 0.25$; $l/h = 2$ and $h/H = 0.5$; $l/h = 0.5$. The numerical results show a higher Nusselt number for the $0.5H$ bar height. A bar geometry with $h/H = 0.25$ and $l/h = 3$ is the communicating channel from Amon et al. [11]. The model considers a steel bar, but the thermal conductivity of the bar does not have influence on the unsteady temperature field in the channel. The Nusselt number also does not depend on the thermal conductivity of the bar material [22].

The channel Reynolds number Re was varied from 100 to 400. The fully developed air flow through the channel geometry can be numerically modeled through a basic unit, indicated by the dashed line in Fig. 1, containing a single vortex generator.

To verify numerical data Grosse-Gorgemann et al. [23] conducted experimental investigations in a channel with periodically mounted ribs as transverse vortex generators in the Reynolds number range of steady laminar to oscillatory transitional flow. The time and area averaged Nusselt number from experiment and from the simulation for a rib height equal to $0.5H$ and $Re = 500$ gives a deviation of only 2%. The numerical results were obtained with only one periodic length. Up to a Reynolds number of $Re = 400$ three-dimensional effects of the unsteady transitional flow can be neglected for the global heat transfer [23]. For this configuration the transition process started with a single frequency at $Re = 100$.

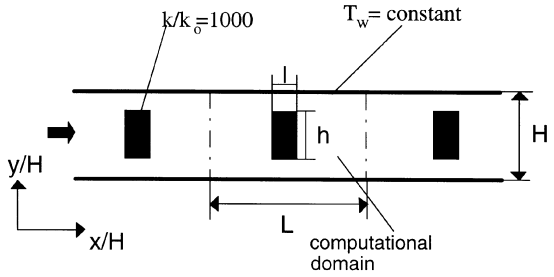

Fig. 1. Computational domain.

The discretization method used in the present study uses a control volume formulation. A detailed description of this discretization method is given by Patankar [24]. Several modifications to the application of SIMPLE method were recommended by van Doormaal and Raithby [25], including the SIMPLEC approximation, TDMA solver and convergence criterion for the pressure equation. These modifications are employed in the present algorithm.

On the rectangular bar, the same governing equations are used. However, the diffusion coefficients in the energy equation are modified to reflect the higher thermal conductivity of the bar material. A zero velocity field on the bar is achieved by adding a source term of very high magnitude in the Navier–Stokes equations in the control volumes where the bar is located.

For the computations a fine grid of 182×82, 342×82 and 502×82 control volumes for $L/H = 2.25$, 4.25 and 6.25, respectively, and time spacing of 0.002 has been used. The time step satisfied the Courant–Friedrich–Levi condition, and approximately 500 time steps are needed for one time period.

The energy equation was solved with the momentum equations for each time step, and a typical run of 30 000 time steps of size equal to 0.002 units of time takes about 10 000 CPU min on an IBM RISC 3BT workstation.

To ascertain the validity of the periodic boundary condition for a computational domain of length $2.25H$, calculations were also performed for a computational domain with two periodic lengths $L = 4.5H$ (two bars) and for a computational domain with three periodic lengths $L = 6.75H$ (three bars) at a Reynolds number of 200. At this Reynolds number the flow is unsteady. The flow structure in two successive periodic regions was anti-symmetric, but the computed differences on the global Nusselt number and Strouhal number between the one and two period cases were less than 5%. The differences on the Nusselt number, Strouhal number and pressure drop between the two and three period cases were less than 2%.

Blancher et al. [26] have investigated the influence of the periodicity hypothesis in a wavy channel. The results show that new unstable modes appear when the geometrical periodicity length increases, with different fundamental frequencies. However, the critical Reynolds number remains approximately constant.

The flow in the channel with the mounted rectangular

bars is dominated from the Karman vortex street. For this reason the influence of other modes from the Tollmien–Schlichting instabilities is less important than in previous works.

To check grid independence, numerical simulations of the unsteady problem with $L/H = 2.25$ and $Re = 200$ were performed on grids of 92×42, 146×66 and 182×82 control volumes. The Strouhal number is a strong function of the numerical damping caused by the grid resolution, therefore the variation of Strouhal number was used to check damping effects of the grid size. The frequency spectra determined with the three grids show Strouhal numbers of 0.912, 0.948 and 0.960, respectively. In spite of these results with the middle grid, the finest grid will be used for all calculations in this paper for the correct simulation of laminar and transitional flows.

4. Results and discussion

The structure of the flow in the periodic region will be discussed. It will be illustrated through the use of computed instantaneous velocity vectors. Figure 2 shows instantaneous maps of fluctuating velocity vectors for different periodicity lengths at $Re = 400$. Note the large recirculation of the unsteady flow in the channel, which exchanges the core fluid with the near-wall fluid. The Karman vortex sheets are alternately shed by the downstream face of the bar and these travel diagonally through the channel, washing across the upstream face of the next bar. Thus, the upstream face of the bar is exposed to a flushing condition induced by the periodic boundary condition.

A fast Fourier transform of the vertical velocity at one point in the computational domain by $L/H = 2.25$ shows that the flow is unsteady with a single dominant shedding frequency that corresponds to a Strouhal number of 0.85 at $Re = 400$, Fig. 3(a). For $Re = 150$ and $Re = 200$ the dominant frequencies correspond to a Strouhal number of 0.96 and at $Re = 100$ the flow is steady.

The flow in the $L/H = 4.25$ arrangement follows a similar qualitative pattern, although the transition Reynolds number for the appearance of the various flow regimes quantitatively differs from those of the $L/H = 2.25$ arrangement. The flow remains steady at $Re = 100$. For $Re = 150$ and 200 the flow is observed to be unsteady with a single dominant shedding frequency or Strouhal number of 0.98. However, for $Re = 300$ additional frequencies appear and a transition to a state with two dominant frequencies is observed by $Re = 400$, Fig. 3(b). In the arrangement with $L/H = 6.25$ the flow characteristics are similar to the case with $L/H = 4.25$. The dominant shedding frequency for $L/H = 6.25$ is, however, much less than for $L/H = 4.25$, Fig. 3(c). It appears that the periodic distance of 4.25 is greater than the bar separation that stabilizes the flow and therefore, delays the transition to turbulence.

The fundamental frequency of the oscillatory flow related to the traveling Tollmien–Schlichting wave associated with the least-stable channel mode for $Re = 400$ is $S = 0.5$ with a length of $2H$ [23]. This suggests that the amplifield instabilities in the arrangements with $L/H > 2$ are Tollmien–Schlichting in nature.

Wang et al. [10] observed that the flow in baffled channels becomes chaotic after the appearance of three incom-

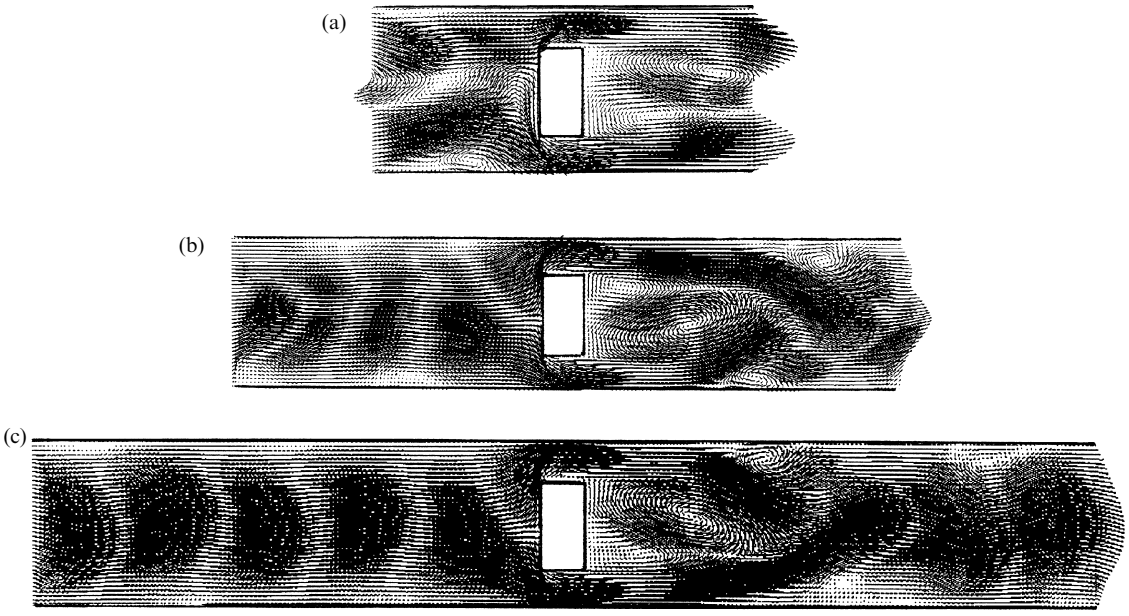

Fig. 2. Instantaneous maps of velocity vectors for the three cases at $Re = 400$: (a) $L/H = 2.25$; (b) $L/H = 4.25$ and (c) $L/H = 6.25$.

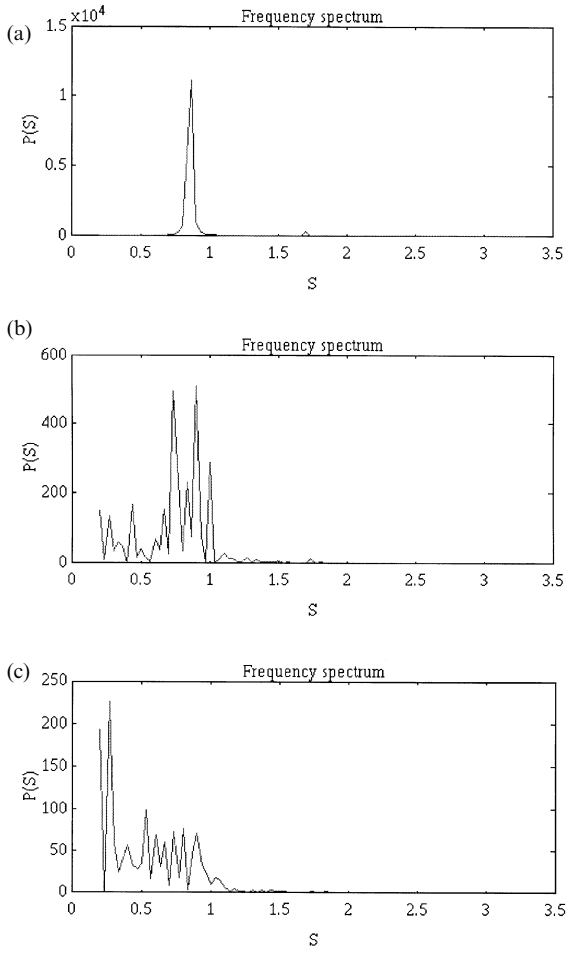

Fig. 3. Power density spectrum of the Strouhal numbers for the vertical velocity for the three cases at $Re = 400$: (a) $L/H = 2.25$; (b) $L/H = 4.25$ and (c) $L/H = 6.25$.

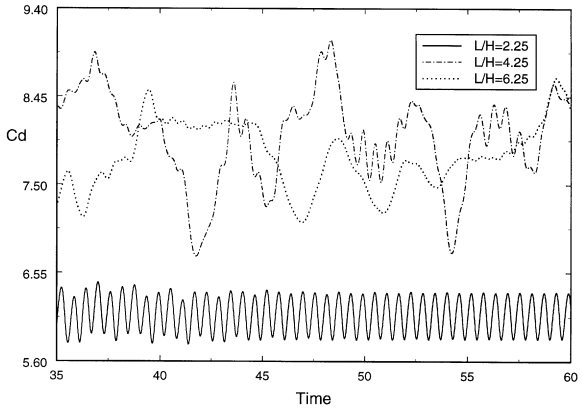

Fig. 4. Temporal variation of the drag coefficient around the rectangular bar at $Re = 400$ for different periodicity lengths.

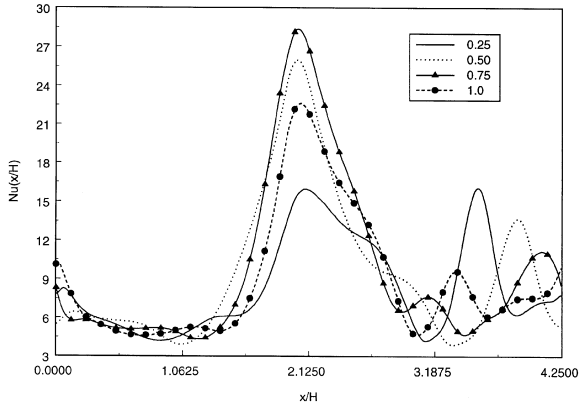

Fig. 5. Instantaneous local Nusselt numbers on the channel wall in a time period for the case $L/H = 4.25$ at $Re = 400$.

mensurate frequencies, following the Ruelle–Takens–Newhouse scenario, a similar scenario is postulated in this geometry. The results presented in Fig. 3 indicate that the flow experiences two successive supercritical Hopf bifurcations, from a laminar steady to a periodic flow with one fundamental frequency, and to a quasiperiodic flow with two dominant frequencies and with more present frequencies.

Figure 4 shows the influence of vortex sheets that are alternately shed by the bar on computed instantaneous drag coefficient at Reynolds number of 400. The instantaneous drag coefficient is periodic for $L/H = 2.25$. For $L/H = 4.25$ and 6.25 the drag coefficients show the characteristics of these transitional unsteady flows. Drag in the arrangements with $L/H > 2$ is increased strongly due to the greater instability of the transverse vortices, Fig. 2.

Figure 5 shows the influence of the unsteady transverse vortices on computed instantaneous local Nusselt numbers at the bottom channel wall observed in a sequence of four time frames within one flow cycle. The local variations are due the unsteady 'washing' of the wall by the oscillating transverse vortices shown in Fig. 2(b).

The temporal variation of the average Nusselt number on the channel bottom wall with different periodicity lengths at $Re = 400$ is shown in Fig. 6. As in the case of drag it is observed that the Nusselt numbers are periodic for the arrangement with $L/H = 2.25$, the amplitude of the oscillation is about 46% of the mean value. With periodicity lengths of $L/H = 4.25$ and 6.25 the temporal variations of the Nusselt numbers are non-periodic, as behavioral consequence of these transitional unsteady flows.

Figure 7 compares the average Nusselt number on the channel walls against the Reynolds number with different periodicity lengths. The increase in the periodicity lengths lead to lower heat transfer in all the flow regimes studied here. The greater heat transfer coefficients are obtained

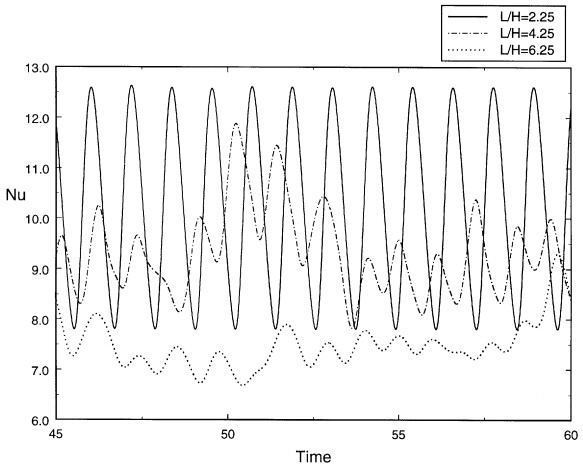

Fig. 6. Temporal variation of the average Nusselt numbers on the channel wall at $Re = 400$ for different periodicity lengths.

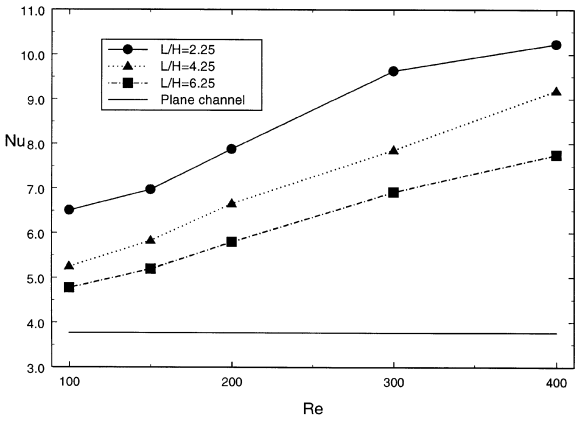

Fig. 7. Time-average Nusselt numbers for different periodicity lengths.

for a periodicity length of 2.25. At $Re = 400$ the Nusselt number is a factor of 2.7 over the Nusselt number in a plane channel. With steady flow ($Re = 100$) the heat transfer enhancement over the plane channel is 73%.

In the arrangement with $L/H = 2.25$ the interaction between the bars is stronger than in the others, although for this periodicity length the flow is periodic with a single dominant shedding frequency at $Re = 400$. This interaction is responsible for high heat transfer augmentation.

The onset of favorably uncoupled heat/momentum transport would explain that the arrangement with $L/H = 6.25$ the Nusselt number is much greater than in the case of plane channel. The pressure gradient, which uncouples the heat and momentum transport mechanisms, merges back to the plane channel value far more rapidly than the dimensionless temperature [27].

The friction factor in the channel with different periodicity lengths versus Reynolds number is shown in Fig. 8. The rectangular bars increase the friction factor in the channel substantially, and the dependency of the friction factor with Reynolds number is nearly the same for all L/H. The periodicity length 6.25 leads to a lower pressure drop due the lower interaction between the bars.

Data for heat transfer in the channel with bars, channel with louver fins and offset fins from [28] were compared with the heat transfer in a laminar and turbulent flow in a plane channel as a function of the dimensionless pumping power $\phi = f \cdot Re^3$ (Fig. 9).

These ordered oscillatory flows require less pumping power than turbulent flows to achieve the same transport rates, because these laminar self-sustained oscillations yield less viscous dissipation than random chaotic turbulent fluctuations, and thereby require less pumping power to reach the same transport rates (Fig. 9). The

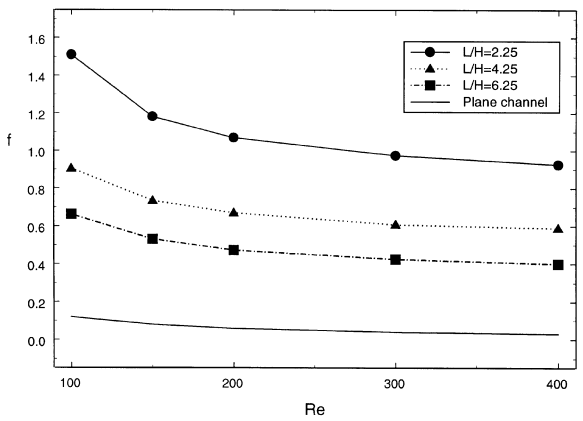

Fig. 8. Time-average friction factor for different periodicity lengths.

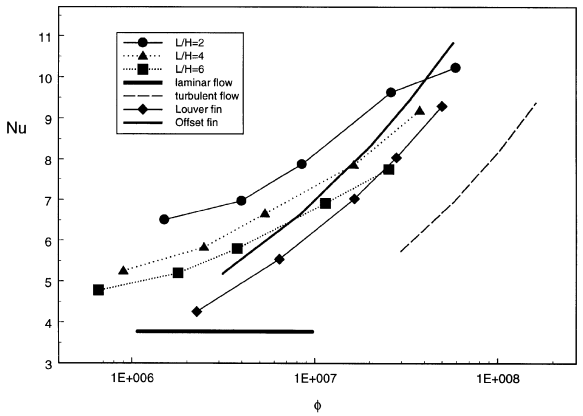

Fig. 9. Comparison of Nusselt numbers as a function of the pumping power for different configurations. Data for louver fin, offset fin and turbulent plane channel from [28].

performance of the investigated channels with mounted bars is better than the channels with offset fins and with louver fins for low pumping power.

5. Conclusions

In this paper, numerical simulations to explore the fluid flow and heat transfer in channels with periodically mounted transverse vortex generators have been employed. The effects of unsteady vortex shedding have been captured by solving the Navier–Stokes and energy equations in two dimensions. Computations were made for three periodicity lengths and for different channel Reynolds numbers. The numerical results reveal the oscillatory structure of the flow when the system is operated near a critical channel Reynolds number of 150. At Reynolds numbers greater than 200 the flow becomes unsteady with several frequencies for periodicity lengths greater than 2.25.

As a consequence of the self-sustained oscillations, there is enhanced mixing between the core fluid and the fluid near the walls. The rates of heat transfer are significantly enhanced, proving this geometry to be attractive as compact heat exchanger.

Acknowledgements

The author gratefully acknowledges the support of this work by the VOLKSWAGEN-Stiftung through a bilateral project with Prof. M. Fiebig, Institut für Thermo- und Fluiddynamik, Ruhr-Universität Bochum, Germany.

References

[1] M. Fiebig, Vortex generators for compact heat exchangers, Journal of Enhanced Heat Transfer 2 (1995) 43–61.
[2] B.R. Noack, H. Eckelmann, A low-dimensional Galerkin method for the three-dimensional flow around a circular cylinder, Physic of Fluids 6 (1994) 124–143.
[3] D.G. Thomas, Forced convection mass transfer: Part II—effect of wires located near the edge of the laminar boundary layer on the rate of forced convection from a flat plate, A.I.Ch.E. Journal 11 (1965) 848–852.
[4] D.G. Thomas, Forced convection mass transfer: Part III—increased mass transfer from a flat plate caused by the wake from cylinders located near the edge of the boundary layer, A.I.Ch.E. Journal 12 (1966) 124–130.
[5] J.S. Kapat, J. Ratnathicam, B.B. Mikic, Experimental determination of transition to turbulence in a rectangular channel with eddy promoters, Journal of Fluids Engineering 116 (1994) 484–487.
[6] G. Karniadakis, B.B. Mikic, A.T. Patera, Minimum-dissipation transport enhancement by flow destabilization: Reynolds' analogy revisited, Journal of Fluid Mechanics 192 (1988) 365–391.
[7] N.K. Anand, C.D. Chin, J.G. McMath, Heat transfer in rectangular channels with a series of normally in-line positioned plates, Numerical Heat Transfer A 27 (1995) 19–34.
[8] M. Greiner, An experimental investigation of resonant heat transfer enhancement in grooved channels, International Journal of Heat and Mass Transfer 34 (1991) 1383–1391.
[9] A. Grosse-Gorgemann, D. Weber, M. Fiebig, Experimental and numerical investigation of self-sustained oscillations in channels with periodic structures, Experimental Thermal and Fluid Science 11 (1995) 226–233.
[10] G. Wang, K. Stone, S.P. Vanka, Unsteady heat transfer in baffled channels, Journal of Heat Transfer 118 (1996) 585–591.
[11] C.H. Amon, D. Majumdar, C.V. Herman, F. Mayinger, B.B. Mikic, D.P. Sekulic, Numerical and experimental studies of self-sustained oscillatory flows in communicating channels, International Journal of Heat and Mass Transfer 35 (1992) 3115–3129.
[12] K. Suzuki, G.N. Xi, K. Inaoka, Y. Hagiwara, Mechanism of heat transfer enhancement due to self-sustained oscillation for an in-line fin array, International Journal of Heat and Mass Transfer 37 (1994) 83–96.
[13] D. Majumdar, C.H. Amon, Oscillatory momentum transport mechanisms in transitional complex geometry flows, Journal of Fluids Engineering 119 (1997) 29–35.
[14] C. Herman, E. Kang, M. Wetzel, Expanding the applications of holographic interferometry to the quantitative visualization of oscillatory thermofluid processes using temperature as tracer, Experiments in Fluids 24 (1998) 431–446.
[15] L.W. Zhang, S. Balachandar, D.K. Tafti, F.M. Najjar, Heat transfer enhancement mechanisms in inline and staggered parallel-plate fin heat exchangers, International Journal of Heat and Mass Transfer 40 (1997) 2307–2325.
[16] L.W. Zhang, D.K. Tafti, F.M. Najjar, S. Balachandar, Computations of flow and heat transfer in parallel-plate fin heat exchangers on the CM-5: effects of flow unsteadiness and three-dimensionality, International Journal of Heat and Mass Transfer 40 (1997) 1325–1341.
[17] H. Suzuki, Y. Inoue, T. Nishimura, K. Fukutani, K. Suzuki, Unsteady flow in a channel obstructed by a square rod (crisscross motion of vortex), International Journal of Heat and Fluid Flow 14 (1993) 2–9.
[18] K. Tatsutani, R. Devarakonda, J.A.C. Humphrey, Unsteady flow and heat transfer for cylinder pairs in a channel, International Journal of Heat and Mass Transfer 36 (1993) 3311–3328.
[19] A. Valencia, Numerical study of self-sustained oscillatory flows and heat transfer in channels with a tandem of transverse vortex generators, Heat and Mass Transfer 33 (1998) 465–470.
[20] S.V. Patankar, C.H. Liu, E.M. Sparrow, Fully developed flow and heat transfer in ducts having streamwise-periodic variations of cross-sectional area, Journal of Heat Transfer 99 (1977) 180–186.
[21] S.V. Patankar, C. Prakash, An analysis of the effect of plate

thickness on laminar flow and heat transfer in interrupted-plate passages, International Journal of Heat and Mass Transfer 24 (1981) 1801–1810.

[22] A. Valencia, Heat transfer enhancement in a channel with a built-in rectangular cylinder, Heat and Mass Transfer 30 (1995) 423–427.

[23] A. Grosse-Gorgemann, H.W. Hahne, H. Neumann, D. Weber, M. Fiebig, Flow and heat transfer in ribbed channels with self-sustained oscillating transverse vortices, Notes on Numerical Fluid Mechanics, vol. 63, Vieweg, Germany, 1998, pp. 131–168.

[24] S.V. Patankar, Numerical Heat Transfer and Fluid Flow, Hemisphere, Washington, DC 1980.

[25] J.P. Van Doormaal, G.D. Raithby, Enhancements of the SIMPLE method for predicting incompressible fluid flows, Numerical Heat Transfer 7 (1984) 147–163.

[26] S. Blancher, R. Creff, P. Le Quere, Effect of Tollmien–Schlichting wave on convective heat transfer in a wavy channel—Part I: linear analysis, International Journal of Heat and Fluid Flow 19 (1998) 39–48.

[27] M. Greiner, R.F. Chen, R.A. Wirtz, Augmented heat transfer in a recovery passage downstream from a grooved section: an example of uncoupled heat/momentum transport, Journal of Heat Transfer 117 (1995) 303–308.

[28] W.M. Kays, A.L. London, Compact Heat Exchangers, 3rd edn., McGraw-Hill, New York, 1984.